Original Research

PLA-based core-shell structure stereocomplexed nanoparticles with enhanced loading and release profile of paclitaxel

Yuemin Wang[1], Siyuan Cui[1], Bing Wu[1], Quanxing Zhang[1], Wei Jiang[1,*]

[1]*State Key Laboratory of Pollution Control and Resources Reuse, National Engineering Research Center for Organic Pollution Control and Resource Reuse, School of the Environment, Nanjing University, 210023 Nanjing, Jiangsu, China*

TABLE OF CONTENTS

1. Abstract

Purpose: In the present study, to achieve high paclitaxel (PTX) loading in a conjugated drug delivery system with minimal long-term side effects, we formulated a novel degradable stereocomplexed micelle-like particle with a core-shell structure. **Materials and methods**: In this system, methoxy polyethylene glycol (MPEG) acted as the hydrophilic shell, and the stereocomplex of polylactic acid with PTX (SCPLA-PTX) acted as the hydrophobic core. The MPEG-SCPLA-PTX micelle-like particles were synthesized via the self-assembly of a MPEG-poly $_L$-lactic acid (PLLA) copolymer with a PTX-poly $_D$-lactic acid-PTX copolymer. The resultant copolymers and their intermediates were characterized using ^{1}H nuclear magnetic resonance and GPC. Micelle-like particles with different molecular weight ratios of MPEG and PLLA were synthesized to demonstrate the functions of both components. **Results**: PTX loading into MPEG2000Da-PLLA6000Da particles reached as high as 20.11%. At 216 h, the cumulative release from MPEG5000Da-PLLA6000Da, MPEG2000Da-PLLA6000Da, and MPEG5000Da-PLLA22000Da particles were 51.5%, 37.7%, and 52.0%, respectively. **Conclusions**: According to the cell uptake experiments, inhibition of tumor cell growth was satisfactory, indicating that the stereocomplexed particles developed in the present study can be employed as a promising nanocarrier for PTX delivery.

2. Introduction

Paclitaxel (PTX) is a tetracyclic diterpene compound that exhibits considerable antineoplastic activity against various solid tumors, including ovarian cancer [1], breast cancer [2, 3], head and neck carcinomas [4, 5], and non-small cell lung cancers [6]. However, it can easily undergo oxidation, and storage is difficult. Its poor water solubility (<1 mg/mL) limits its uptake in the human body [7]. Furthermore, PTX fails to meet current patient needs because of its limited extraction efficiency from the bark of the yew tree (0.04% [w/w]) [8]. Therefore, increasing the utilization of PTX has become an urgent goal in pharmaceutical research [9, 10]. Taxol® is a relatively well-developed PTX injectable formulation using polyoxyethylene castor oil and ethanol as co-solvents; these solvents increase the solubility and stability of PTX [11]. However, when used clinically, the stability of PTX in the formulation deteriorates after dilution with saline or glucose [12]. One considerable problem is that polyoxyethylene castor oil reportedly releases histamine and facilitates the degradation of pharmaceutical formulations, which could result in severe allergic reactions [13].

Several types of PTX formulations are available, including liposomes [14, 15], cyclodextrin inclusion compounds [16, 17], PTX prodrugs [18–20], PTX nanoparticles, and microspheres [21]. Notably, amphiphilic poly-

Submitted: 8 July 2021 Revised: 5 August 2021 Accepted: 27 August 2021 Published: 30 September 2021

mer particles have attracted considerable research interest in pharmaceutical formulation development owing to their excellent performance as drug carriers [22]. Amphiphilic macromolecule polymers can readily self-assemble in aqueous solution to form nanoparticles with a hydrophobic inner core and hydrophilic shell, encapsulating lipophilic drugs in the hydrophobic core to increase drug solubility owing to the lower critical micelle concentration (CMC) of amphiphilic macromolecule polymers [23]. The hydrophilic shell also protects particles from being recognized by the reticuloendothelial system and removal from the body [24]. Polyethylene glycol–polylactic acid (PEG-PLA) is an amphiphilic biodegradable material approved by the U.S. Food and Drug Administration (FDA) for biomedical applications and is widely used as a pharmaceutical drug carrier [25, 26]. We selected MPEG-PLLA as the target product to achieve green and controllable synthesis.

Amphiphilic PEG-PLA chains are used as carriers of PTX; however, the drug loading content is limited by the compatibility between drug molecules and the hydrophobic PLA segment, resulting in undesirable rapid drug release [27–30]. For chemical cross-linking methods, such as linking by ester bonds, the complex architecture of polymers tends to increase synthetic difficulties. The introduction of harmful and non-degradable ingredients is inevitable, which results in long-term systemic side effects [31, 32]. A biodegradable stereocomplex composed of polylactic acid (SCPLA) is formed by the selective combination of dextral polylactic acid (PDLA) and levo-polylactic acid (PLLA) molecular chains. A few researchers have previously explored its potential application in drug delivery [33, 34] and obtained satisfactory results. In our designed micelle-like particles, we chemically linked PTX to PDLA and utilized the stereocomplex structure to combine it with methoxy poly (ethylene glycol)-PLLA (MPEG-PLLA). Accordingly, we achieved a relatively high PTX-loading efficiency using biodegradable PLA-based particles.

In the present study, MPEG-SCPLA-PTX particles were synthesized via a two-step self-assembly process. In the first step, PTX-PDLA-PTX and MPEG-PLLA formed MPEG-SCPLA-PTX through the stereocomplex formed by PDLA and PLLA. In the second step, MPEG-SCPLA-PTX self-assembled into particles under a hydrophobic effect. Characterization and tumor cell inhibition tests confirmed the successful chemical embedding of PTX into particles and the effectiveness of MPEG-SCPLA-PTX particles.

3. Materials and methods

3.1 Materials

MPEG (molecular weight: 5000 Da and 2000 Da) was purchased from Sigma-Aldrich (Burlington, VT, USA). l-lactide (LLA) was purchased from Shenzhen Esun Industrial Co. Ltd. (Shenzhen, China), and PTX was obtained from J&K Scientific Ltd. (Guangzhou, China). Tetrahydrofuran (THF) was purchased from Tianjin Kemi Europe Chemical Reagent Co., Ltd. (Tianjin, China). Diethyl ether, succinic anhydride (99%), *N*,*N*-dimethylpyridin-4-amine (DMAP; 99%), and DCC (99%) were obtained from Alfa Aesar (Shanghai, China). $Zn(Oct)_2{\cdot}2H_2O$, n-hexane, acetone, HCl, and $MgSO_4$ were purchased from Aladdin (Shanghai, China), and d-lactic acid (90 wt%) was purchased from Musashino Chemical Co., Ltd. (Yichun, China). Phosphate-buffered saline (PBS; pH 7.4, 1×) was purchased from Gibco (New York, NY, USA). A dialysis bag (MWCO = 2500 Da, composition: reborn cellulose fiber) was obtained from Viskase (Chicago, IL, USA). HeLa cells and the 5,5,6,6-Tetrachloro-1,1,3,3-tetraethylbenzimidazolylcarbocyanine iodide (JC-1) detection kit were obtained from KeyGEN Biotech (Nanjing, China). Cell Counting kit-8 (CCK-8) and calcein-AM (CAM) were obtained from Dojindo Molecular Technologies (Kumamoto, Japan). 2, 7-Dichlorofluorescein diacetate (DCF) was purchased from Life Technologies (Carlsbad, CA, USA). Hoechst 33342 was purchased from YeaSen Biotechnology (Shanghai, China). All reagents were of analytical grade, and all solutions were prepared with deionized water (DI) without further purification.

3.2 Synthesis of MPEG-PLLA

As shown in Fig. 1a, MPEG-PLLA copolymers were synthesized via ring-opening polymerization (ROP) [35]. l-lactide and MPEG were used as raw materials for the synthesis of amphiphilic diblock copolymers. The molecular weight of the MPEG-PLLA copolymer was regulated by the molar ratio of the monomers (molecular weight and ratio are listed in **Supplementary Table 1** in the **Supplementary material**). A specific amount of MPEG, LLA, and $Zn(Oct)_2{\cdot}2H_2O$ were added to a flame-dried and argon-purged flask. The flask was evacuated and charged with argon three times and sealed under a vacuum and subjected to magnetic stirring. After the mixture was stirred at 150 °C for 15 h, the synthesized polymer was recovered by dissolving it in methylene chloride, followed by precipitation in ice-cold diethyl ether. The resultant precipitate was filtered and dried at 40 °C under a vacuum for 48 h. MPEG-PLLA with different molecular weights of MPEG and PLLA are named $MPEG_{5000}$-$PLLA_{6000}$, $MPEG_{2000}$-$PLLA_{6000}$, and $MPEG_{5000}$-$PLLA_{2000}$.

3.3 Synthesis of PTX-PDLA-PTX

Synthesis route for PTX-PDLA-PTX is shown in Fig. 1b. The typical procedure was as follows: 230 g of d-lactic acid was added to a four-necked flask. The flask equipped with a mechanical stirrer and reflux condenser was connected to a vacuum-argon system, and the flask was evacuated and charged with argon three times. The mixture

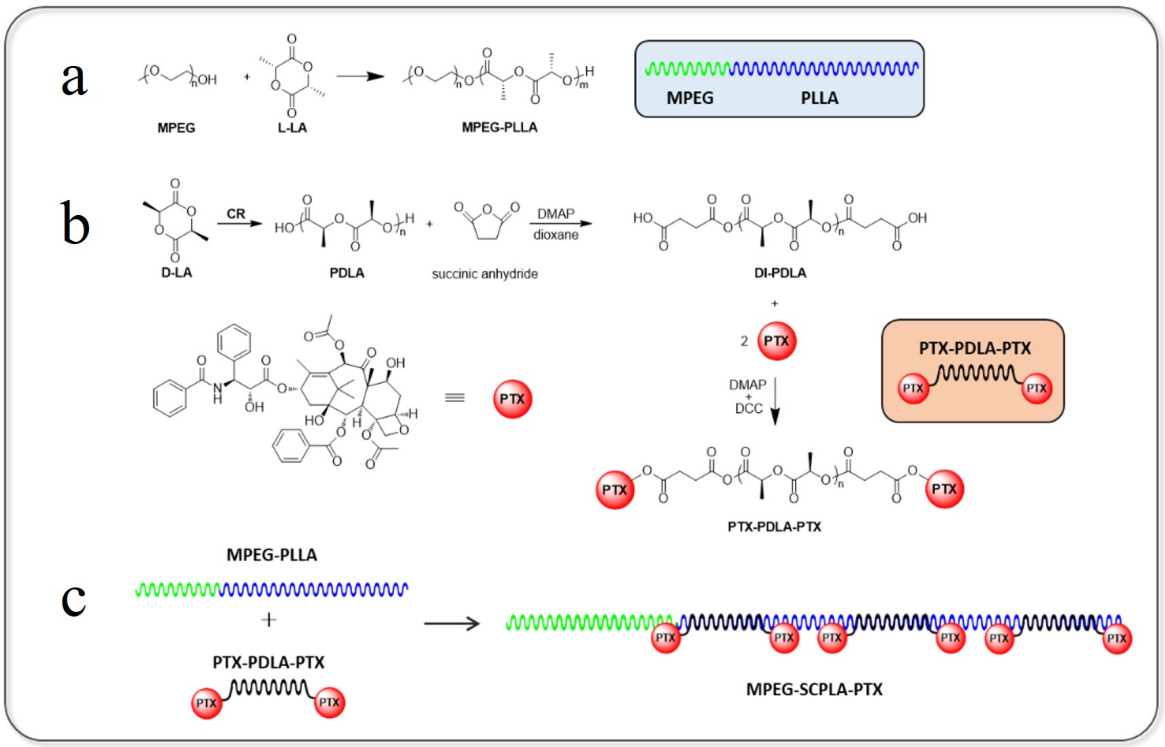

Fig. 1. Synthesis route for the formation of (a) MPEG-PLLA, (b) PTX-PDLA-PTX, and (c) MPEG-SCPLA-PTX particles.

was heated to 100 °C and then reduced to 400 Torr for 3 h. Next, the mixture was heated to 130 °C under a successively reduced pressure of 100 Torr for 3 h. The reaction was maintained under these conditions for an additional 3 h. The resultant mixture was heated to 150 °C, and the system pressure was successively reduced to 10 Torr over 6 h. The flask was cooled to 25 °C at the end of the polymerization process. The contents were dissolved in acetone, and the solution was poured into cold water. The precipitate was collected and dried under a vacuum for 48 h at 40 °C to yield a white solid. ($M_{n,NMR}$ = 1950 g/mol, $M_{n,GPC}$ = 2140 g/mol, M_w/M_n = 1.35, where M_n refers to number average molecular weight, M_w refers to weight average molecular weight).

Purified PDLA (3 g, 1.5 mmol), succinic anhydride (0.3002 g, 3 mmol), and DMAP (0.3665 g, 3 mmol) were dissolved in 1, 4-dioxane (20 mL) and reacted in a nitrogen atmosphere for 48 h at room temperature. The product was precipitated in n-hexane, and the polymer precipitate was dried under a vacuum for 48 h at room temperature. The polymer was reconstituted using THF and poured into a large amount of distilled water. The resultant precipitate was filtered and dried under vacuum at room temperature for 48 h. A dicarboxylic PDLA (DI-PDLA) with terminal carboxyl groups was obtained. ($M_{n,NMR}$ = 2100 g/mol, $M_{n,GPC}$ = 2770 g/mol, Mw/Mn = 1.16).

DI-PDLA (0.222 g) and PTX (126.5 mg) were dissolved in anhydrous methylene chloride (30 mL) in a dried flask. DCC (30.6 mg) and DMAP (18.1 mg) were added at 0 °C. The reaction mixture was stirred for 48 h at 0 °C. The precipitate was filtered out, and the filtrate was washed with 0.1 mol/L HCl and water. The organic phase was dried over anhydrous $MgSO_4$. Methylene chloride was removed under a vacuum. ($M_{n,NMR}$ = 3300 g/mol, $M_{n,GPC}$ = 3970 g/mol, M_w/M_n = 1.14).

3.4 Preparation of MPEG-SCPLA-PTX particles

Synthesis route for MPEG-SCPLA-PTX particles is shown in Fig. 1c. PTX-loaded particles were prepared using a solvent displacement method with a THF/H_2O system. In a 100 mL volumetric flask, MPEG-PLLA (22 mg, 0.002 mmol) and PTX-PDLA-PTX (19.8 mg, 0.006 mmol) were first dissolved in THF (10 mL) for 3 h using a magnetic stirring bar. Thereafter, 40 mL of doubly distilled water was added with gentle agitation for 6 h. Finally, THF was slowly removed at ambient temperature for 1 h by rotary evaporation to obtain the particles. Particles obtained from $MPEG_{5000}$-$PLLA_{6000}$, $MPEG_{2000}$-$PLLA_{6000}$, and $MPEG_{5000}$-$PLLA_{2000}$ were named 5-6, 2-6, and 5-2 particles.

Blank particles were prepared in a manner similar to PTX-loaded particles. MPEG-PLLA (22 mg, 0.002 mmol) and DI-PDLA (12.6 mg, 0.006 mmol) were first dissolved in THF (10 mL), and the following steps were identical to those previously described.

3.5 Characterization

GPC measurements were conducted using a PL-GPC120 instrument (Polymer Laboratories, Shropshire,

UK) equipped with an Agilent MIXED-B column and a differential refractometer detector. THF (with 0.02–0.03 wt% BHT stabilizer) was used as the eluent and maintained at a flow rate of 1 mL/min at 40 °C. Nuclear magnetic resonance (^{1}H-NMR) spectra were measured using a Bruker DRX-400 spectrometer (Bruker, Bremen, Germany) in $CDCl_3$ at 25 °C. Chemical shifts are reported in parts per million using tetramethylsilane as an internal reference. Thermograms were obtained using a Q2000-2460DSC instrument (TA, Lindon, UT, USA). The lyophilized sample powder (3–5 mg) was crimped in standard aluminum pans and heated from 25 °C to 230 °C at a speed of 10 °C/min, cooled from 230 °C to 0 °C at a rate of 10 °C/min, and heated from 0 °C to 230 °C at a speed of 10 °C/min. SEM analyses were performed using an S-4800 scanning electron microscope (Hitachi, Tokyo, Japan) at an acceleration voltage of 10 kV. TEM analyses were performed using a JEM-200CX transmission electron microscope (JEOL, Tokyo, Japan) at an acceleration voltage of 100 kV. The hydrodynamic radius and size distribution of the particles were determined via dynamic light scattering (DLS) (Zetasizer Nano ZS90, Malvern, UK) with a scattering angle of 90°.

3.6 Calculation of drug content

The drug loading efficiency (LE) was calculated as follows:

$$\text{Loading Efficiency (\%)} = \frac{\text{total paclitaxel amount-free paclitaxel amount}}{\text{amount of paclitaxel loaded micelle}} \times 100\% \quad (1)$$

The calculation formula could be further specified to:

$$\text{LE} = \frac{\text{M}_{\text{n,PTX-PDLA-PTX}} - \text{M}_{\text{n,DI-PDLA}}}{\text{M}_{\text{n,PTX-PDLA-PTX}}} \times 100\% \quad (2)$$

where $M_{n,PTX-PDLA-PTX}$ and $M_{n,DI-PDLA}$ are the average molecular weights calculated by ^{1}H-NMR (**Supplementary Table 2**).

Based on the dosages of MPEG-PLLA and PTX-PDLA-PTX (**Supplementary Table 5**), the total theoretical PTX loading of the particles can be calculated as:

$$\text{TTLE} = \frac{\text{LE} \times \text{m}_{\text{PTX-PDLA-PTX}}}{\text{m}_{\text{MPEG-PLLA}} + \text{m}_{\text{PTX-PDLA-PTX}}} \times 100\% \quad (3)$$

Physical embedding ratio can be calculated as:

$$\text{Physical embedding ratio} = \frac{\text{m}_{\text{PTX-HPLC}}}{3\text{mg} \times \text{TTLE}} \times 100\% \quad (4)$$

where $m_{PTX-HPLC}$ is the PTX content measured by HPLC, 3 mg is the mass of particles used for analysis, and TTLE is the theoretical total drug loading. The dosing quantities of PTX-PDLA-PTX ($m_{PTX-PDLA-PTX}$) and MPEG-PLLA ($m_{MPEG-PLLA}$) are shown in **Supplementary Tables 5,6**.

Considering that PTX is loaded only by physical or chemical methods, the chemical embedding ratio is calculated as:

$$\text{Chemical embedding ratio} = (1\text{-Phsical embedding ratio}) \times 100\% \quad (5)$$

3.7 CMC measurements

CMC represents the lowest concentration of the block copolymer required in solution to form polymer micelles [36], which is used to characterize the stability of micelle-like particles. The CMC of the PTX micelle-like particles and blank micelle-like particles was determined using a fluorescence technique with pyrene as a hydrophobic probe. Steady-state fluorescence spectra were obtained using a PerkinElmer LS50B luminescence spectrometer (ALT, Norwalk, CT, USA). A predetermined amount of pyrene solution in acetone was added to a volumetric flask, and the acetone was completely evaporated. The flask containing the solid pyrene was filled with DI water up to the calibration line. The pyrene concentration in the final solution was 12×10^{-7} mol/L (the saturation solubility of pyrene in water at 22 °C was 6×10^{-7} mol/L). Next, sample solutions were prepared by adding the pyrene solution in DI water and predetermined amounts of micelle-like particles to a series of flasks. A series of copolymer concentrations ranging between 10^{-4} and 0.4 g/L was achieved by predetermining the volume of the copolymer solution. The concentration of pyrene in the final solution was 6×10^{-7} mol/L, which is similar to the saturation solubility of pyrene in water at 22 °C. The flasks were thermostated at 40 °C for approximately 2 h to equilibrate the pyrene partition between the water and micelle-like particles and subsequently cooled overnight to room temperature. The emission wavelength was 390 nm, and the excitation bandwidth was 5 nm. The spectra were recorded at a scanning rate of 240 nm/min. Nagasaki *et al.* [37] observed that I335/I333 is equally sensitive to environmental changes and, therefore, can be used to determine polymer CMC. Test solutions were prepared at concentrations of 0.4 g/L, 0.1 g/L, 0.01 g/L, 0.001, 0.002, and 0.0001 g/L.

3.8 *In vitro* release studies

In vitro PTX release from block copolymer particles was investigated in PBS (pH = 7.4) [38]. Typically, 10 mL of 5-6 particles at a concentration of 1.4 mg/mL, 2-6 particles at a concentration of 1.7 mg/mL, and 5-2 particles at a concentration of 1.9 mg/mL were placed in a dialysis bag (MWCO = 2500 Da). The release experiment was initiated by placing the end-sealed dialysis bag in 40 mL PBS solution at 37 °C with continuous shaking at 150 rpm to measure the PTX released from the particles. At a certain interval, samples (40 mL) were withdrawn, and the same volume of fresh buffer medium was replaced. The duration of the *in vitro* release study was 216 h. The concentration of the released PTX in the dialysis medium was determined via HPLC using a C_{18} column at 25 °C and

a Waters Model 2487 UV detector, and a mixture of water/acetonitrile (50:50 v/v) was used as the mobile phase at a flow rate of 1 mL/min at 227 nm. The cumulative amount of PTX released was calculated using a calibration curve and expressed as the percentage of PTX released.

3.9 Tumor cell inhibition tests

3.9.1 Cell culture

HeLa cells were maintained in modified Eagle's medium (MEM) with 10% fetal bovine serum (FBS) under standard cell culture conditions (37 °C and 5% CO_2). Prior to treatment with PTX and PTX-loaded particles, HeLa cells at a density of 100,000 cells/well were allowed to attach in 96-well plates for 24 h. Next, the cells were exposed to PTX or PTX-loaded particles in MEM medium for 24 h. These were used for further analyses.

3.9.2 Cell viability

The viability of HeLa cells was determined using CCK-8 assay. MK571 and PSC833 (10 mM), known inhibitors of multidrug resistance-associated proteins (MRPs/ABCCs), and a subfamily of ATP-binding cassette transporters (ABC transporters), were used as positive controls. After 24 h exposure to different concentrations of PTX-loaded particles, 10 μL of CCK-8 solution was added to each well of the 96-well plate and incubated for 2 h at 37 °C in 5% CO_2. Cell viability was calculated from the relative absorbance at 450 nm using a microplate reader (Synergy H1, Biotek, Beijing, China).

3.9.3 Intracellular reactive oxygen species (ROS) level

Intracellular ROS levels were assessed based on the increased fluorescence values of the DCF cell dye. To reduce errors due to loss of cell numbers during exposure to PTX-loaded particles, Hoechst 33342 (YeaSen Biotechnology, Shanghai, China), a fluorescent dye used to stain DNA, was employed to measure the number of HeLa cells remaining in each well and normalize the DCF fluorescence value. After PTX exposure, DCF (final concentration: 10 μM) was added to each well of a 96-well plate. After incubation for 25 min, the cells were washed with phosphate-buffered saline (PBS). Next, Hoechst 33342 (final concentration: 5 μg/mL) was added, and the cells were incubated for 15 min. The fluorescence values of DCF and Hoechst 33342 were measured using a microplate reader [39, 40]. The excitation and emission wavelengths for DCF were 485 and 530 nm, respectively, and 350 and 460 nm for Hoechst 33342.

3.9.4 Cell apoptosis

Mitochondrial membrane potential, an early indicator of cell apoptosis, was measured using a JC-1 detection kit [41]. After exposure to PTX for 24 h, JC-1 solution (final concentration: 20 nM) was added to each well of a 96-well plate, and the plate was incubated for 25 min. The fluorescence intensity of JC-1 was measured using a microplate reader. Two fluorescence values were observed for JC-1. The excitation and emission wavelengths for green fluorescence were 485 and 530 nm, respectively, and those for red fluorescence were 530 and 590 nm, respectively. The ratio of red to green fluorescence was used to determine the mitochondrial membrane potential.

3.9.5 Cell uptake of drugs

Lysosomes in HeLa cells were determined using LysoTracker Deep Red (Molecular Probes)(Thermo Fisher Scientific, Shanghai, China), which indirectly indicates the cellular uptake of PTX [42]. Similar to the DCF assay, Hoechst 33342 was used to normalize the fluorescence value of LysoTracker. After exposure to PTX for 24 h, LysoTracker solution (final concentration: 50 nM) was added to each well, and the cells were incubated for 30 min. Hoechst 33342 was added and the cells were incubated as described above. Finally, the cells were analyzed using a microplate reader. The excitation and emission wavelengths for LysoTracker were 647 nm and 668 nm, respectively.

3.9.6 Membrane transporter activity

CAM was used to assess ABC transporter activity using a dye accumulation assay [43, 44]. After exposure to PTX for 24 h, CAM at a final concentration of 0.25 μM was added to each well of a 96-well plate. After incubation for 2 h, the cells were washed with Hanks' buffer. Hoechst 33342 was used to normalize the CAM fluorescence values to the cell number. Fluorescence values were measured using a microplate reader. The excitation and emission wavelengths of CAM were 485 and 530 nm, respectively.

4. Results and discussion

4.1 Characterization of MPEG-PLLA, PTX-PDLA-PTX, and MPEG-SCPLA-PTX

In the present study, MPEG reacted completely without residual monomers, as the characteristic MPEG peak was not observed in the GPC traces (Fig. 2a,b). A single peak with a relatively narrow distribution indicates the successful synthesis of MPEG-PLLA, DI-PDLA, and PTX-PDLA-PTX (Fig. 2).

The ^{1}H-NMR spectra of MPEG, PLLA, and MPEG-PLLA are shown in Fig. 3. The existence of the characteristic peak of MPEG (a, b), as well as the characteristic peak of PLLA (c, d), indicate the successful synthesis of copolymers.

The ^{1}H-NMR spectra of PDLA and DI-PDLA were compared, as shown in Fig. 4. The characteristic peaks of hydrogen atoms on the CH of the repeating structural units (c' δ = 2.65 ppm) in DI-PDLA revealed that the terminal hydroxyl group of PDLA was converted to carboxyl, and polymer DI-PDLA was obtained. **Supplementary Fig. 1** shows the ^{1}H-NMR spectra of DI-PDLA, PTX,

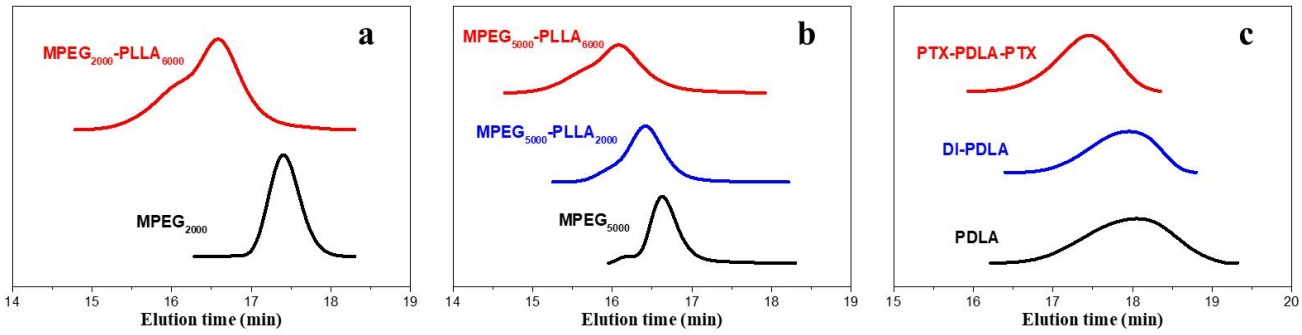

Fig. 2. GPC traces of (a) MPEG2000 and MPEG2000-PLLA6000; (b) MPEG5000, MPEG5000-PLLA2000, and MPEG5000-PLLA6000; (c) PDLA and its derivative. Abbreviation: GPC, gel permeation chromatography.

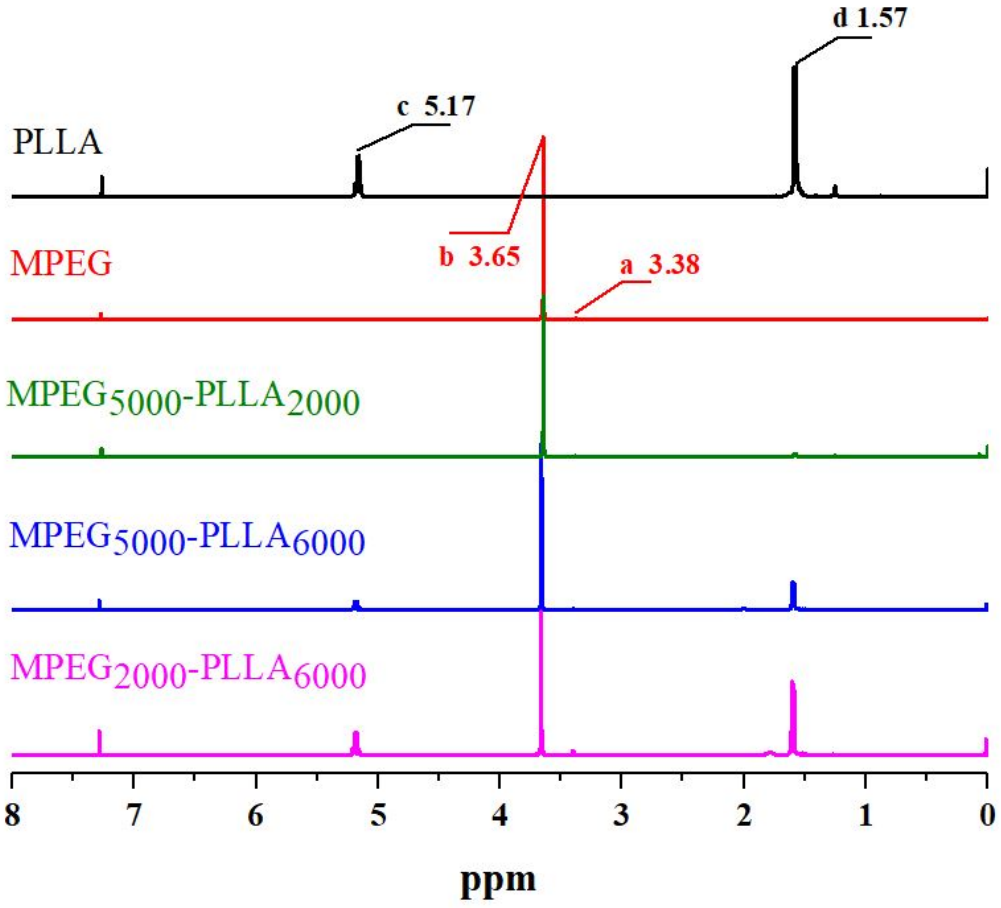

Fig. 3. ^{1}H-NMR spectra of PLLA, MPEG and MPEG-PLLA.

and PTX-PDLA-PTX. Characteristic peaks of both PTX and DI-PDLA were observed in the ^{1}H-NMR spectrum of PTX-PDLA-PTX, indicating the formation of PTX-PDLA-PTX.

The specific molecular weights and distribution coefficients of PDLA and its derivatives are listed in **Supplementary Table 2**. For the molecular weight, a specific difference can be observed between the results calculated from ^{1}H-NMR and the measured values from GPC. This could be attributed to the hydrodynamic gap between PDLA and its derivatives and the GPC standard polystyrene.

The thermodynamic properties of the micelle-like particles and MPEG-PLLA were measured by DSC (Fig. 5), and the results confirmed the self-assembly of enantiomeric PLA-based copolymers. The peak at a relatively high temperature corresponds to the melting point of the PLA chain. Owing to the formation of SCPLA, the melting point of the PLA chain in 5-6 particles and 2-6 particles increased

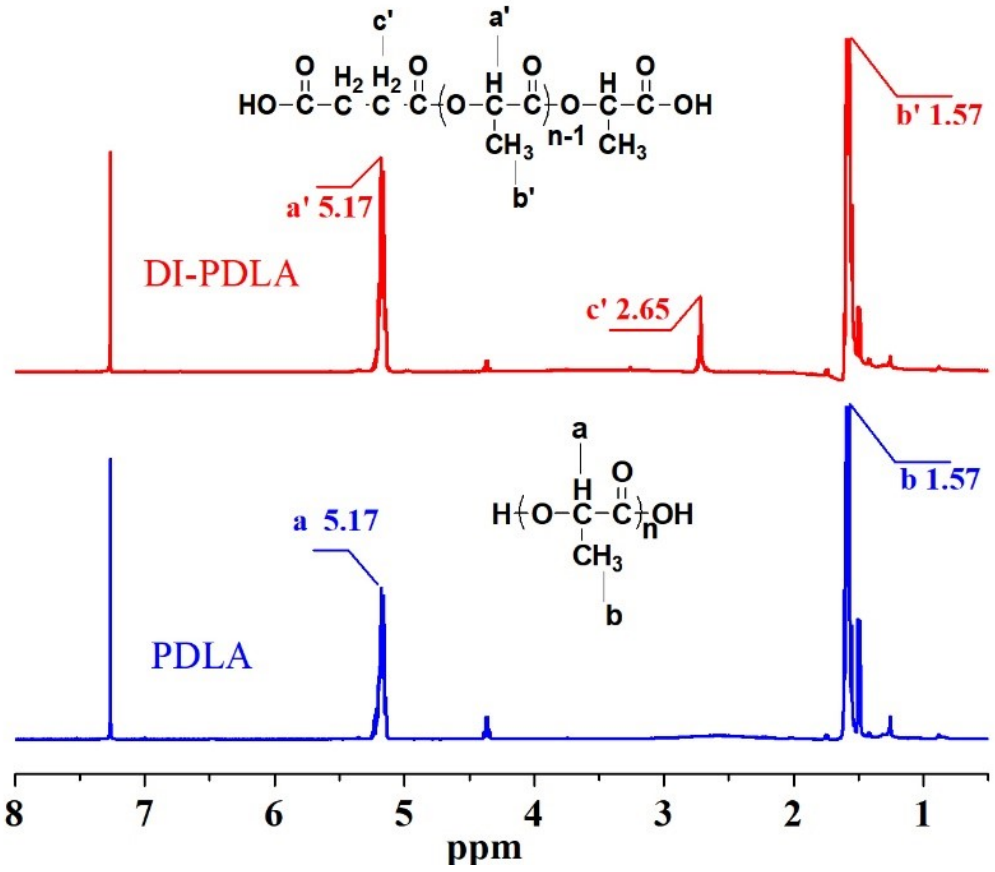

Fig. 4. ^{1}**H-NMR spectra of PDLA and DI-PDLA.**

from 151.6 °C to 191.3 °C and from 143.0 °C to 189.0 °C, respectively, after $MPEG_{5000}$-$PLLA_{6000}$ and$MPEG_{2000}$-$PLLA_{6000}$ self-assembled with PTX-PDLA-PTX (Fig. 5a-b). As shown in Fig. 5c, when $MPEG_{5000}$-$PLLA_{2000}$ reacted with PTX-PDLA-PTX to obtain the SCPLA structure, the melting point of the MPEG segment decreased from 56.7 °C to, 53.2 °C , as the PLLA chain hindered the crystallization process of the MPEG chain. The PLA segment had no melting peak because the PLA segment was markedly short. These results are consistent with previously reported results [45]. For comparison, after $MPEG_{5000}$-$PLLA_{6000}$ reacted with DI-PDLA without PTX, the melting point increased from 142.4 °C to 189.4 °C (Fig. 5d), which was also a great improvement, eliminating the possibility of PTX enhancing the melting point. These results demonstrate that the structure of MPEG-SCPLA-PTX was obtained through the reaction of MPEG-PLLA and PTX-PDLA-PTX or DI-PDLA, linked via the structure of SC in the PLA segment. Polymer particles with a hydrophilic shell were obtained following the solution reaction.

The particle size and distribution of the drug-loaded and blank copolymer particles were investigated by DLS, as shown in Table 1 and Fig. 6. The DLS results of drug-loaded and blank copolymer particles all displayed narrow, single peaks and a normal distribution at a concentration of 0.5 mg/mL, indicating that the particle size distribution was relatively concentrated. The average particle size of 5-6 blank particles, 2-6 particles, 5-6 particles, and 5-2 particles was 78.8 nm, 141.3 nm, 111.4 nm, and 132.4 nm, respectively. The mean particle size of 5-6 blank particles was substantially smaller than that of the other particles owing to a lack of PTX.

The relative molecular ratio of the components in the copolymer demonstrated a marked impact on the micellar size. Comparing 5-6 particles with 2-6 particles, the length of PLA at the hydrophobic end was consistent, and accordingly, the hydrophobic core of the micellar particles was equally large. The 5-6 particles presented a longer MPEG chain that greatly improved the particle hydrophilicity; hence, the particle size was less than that of 2-6 particles (111.4 nm $<$ 141.3 nm). Comparing 5-2 particles with 5-6 particles, the lengths of MPEG at the hydrophilic end were similar. The 5-6 particles had a longer PLA chain where more SCPLA was formed; accordingly, the particle size of 5-6 particles was less than that of 5-2 particles owing to the curling of the chain segments (111.4 nm $<$ 132.4 nm).

TEM images of 5-6 particles, 2-6 particles, 5-2 particles, and 5-6 blank particles are shown in Fig. 7a–d,

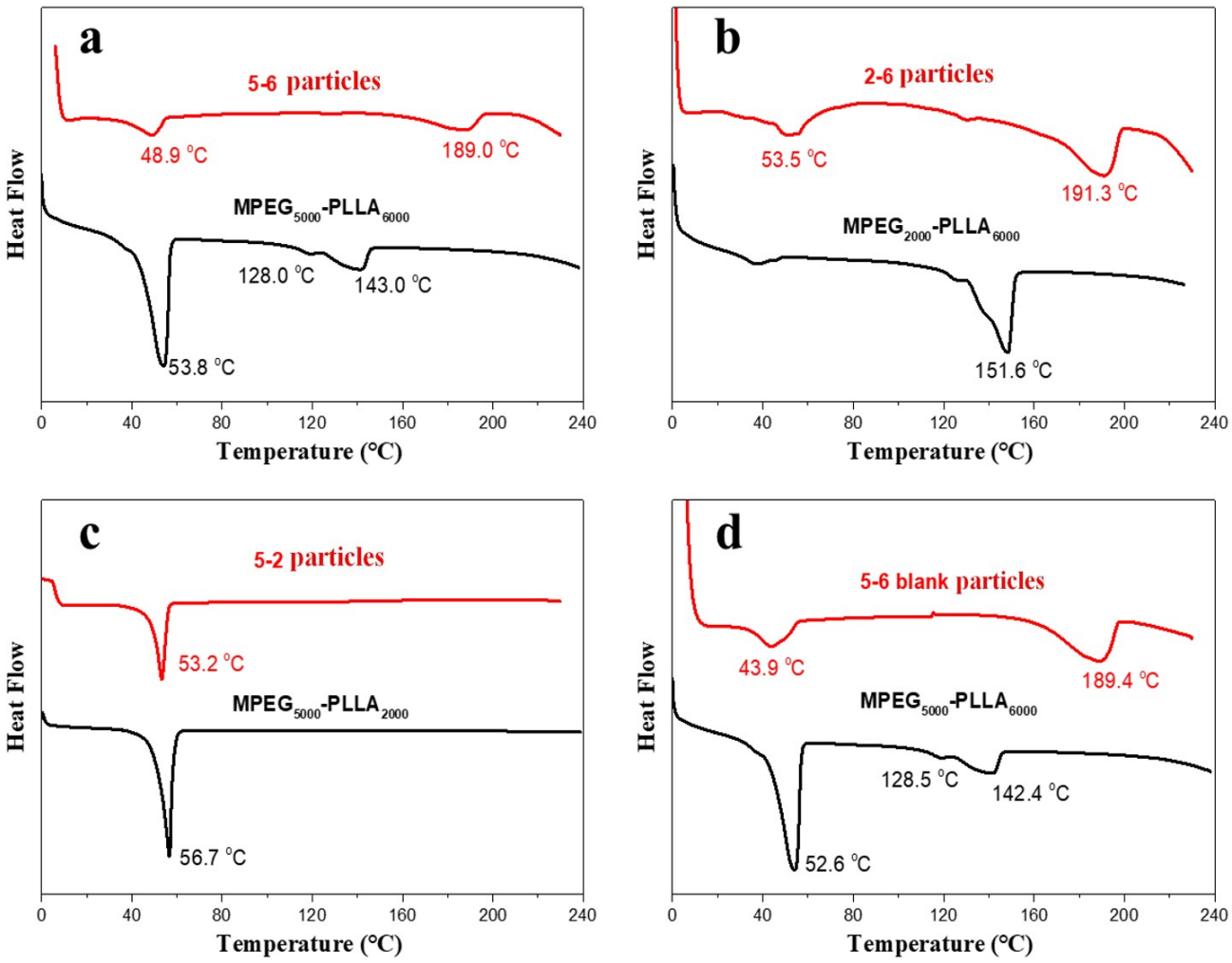

Fig. 5. DSC curves of (a) $MPEG_{5000}$-$PLLA_{6000}$ and 5-6 particles; (b) $MPEG_{2000}$-$PLLA_{6000}$ and 2-6 particles; (c) $MPEG_{5000}$-$PLLA_{2000}$ and 5-2 particles; (d) $MPEG_{5000}$-$PLLA_{6000}$ and 5-6 blank particles. Abbreviation: DSC, differential scanning calorimetry.

Table 1. Particle size and distribution of drug-loaded and blank copolymer particles.

	5-2 particles	5-6 particles	2-6 particles	5-6 blank particles
Average size	132.4 nm	111.4 nm	141.3 nm	78.8 nm

and the SEM images are shown in Fig. 7e–h. The as-formed particles have a spherical morphology with an approximate diameter of 100 nm. The size measured by DLS analysis was slightly larger than that determined by TEM and SEM images, and some particles with diameters larger than 200 nm were observed in the SEM images (Fig. 7g). This could be attributed to the dehydration of the samples during the preparation. Dehydration of the hydrophilic MPEG shell particles resulted in smaller particles. However, micellar aggregation resulted in several larger particles.

4.2 Drug loading analysis of particles

Based on these calculations, the PTX loading efficiencies for different particles are listed in Table 2. The physical loading of PTX in 5-6 particles, 2-6 particles, and 5-2 particles is shown in Table 3. The loading content of PTX in 2-6 particles reached 20.11%. Drug loading ratio of the chemical method On comparing 5-6 particles with 5-2 particles, it was observed that the larger the molecular weight of PLA, the higher the drug loading content of PTX.

4.3 CMC of particles

The fluorescence emission spectra of the pyrene probe in 5-6 particles, 2-6 particles, 5-2 particles, and 5-6 blank particles at different polymer solution concentrations are shown in **Supplementary Fig. 3**. The maximum peak intensity ratio I335/I333 in the excitation spectrum was plotted against the logarithm of the polymer concentration, and each sample exhibited an S-shaped curve, as shown in Fig. 8.

The CMC of drug-loaded 5-6 particles, 2-6 particles, 5-2 particles, and 5-6 blank particles were 1.4×10^{-3}

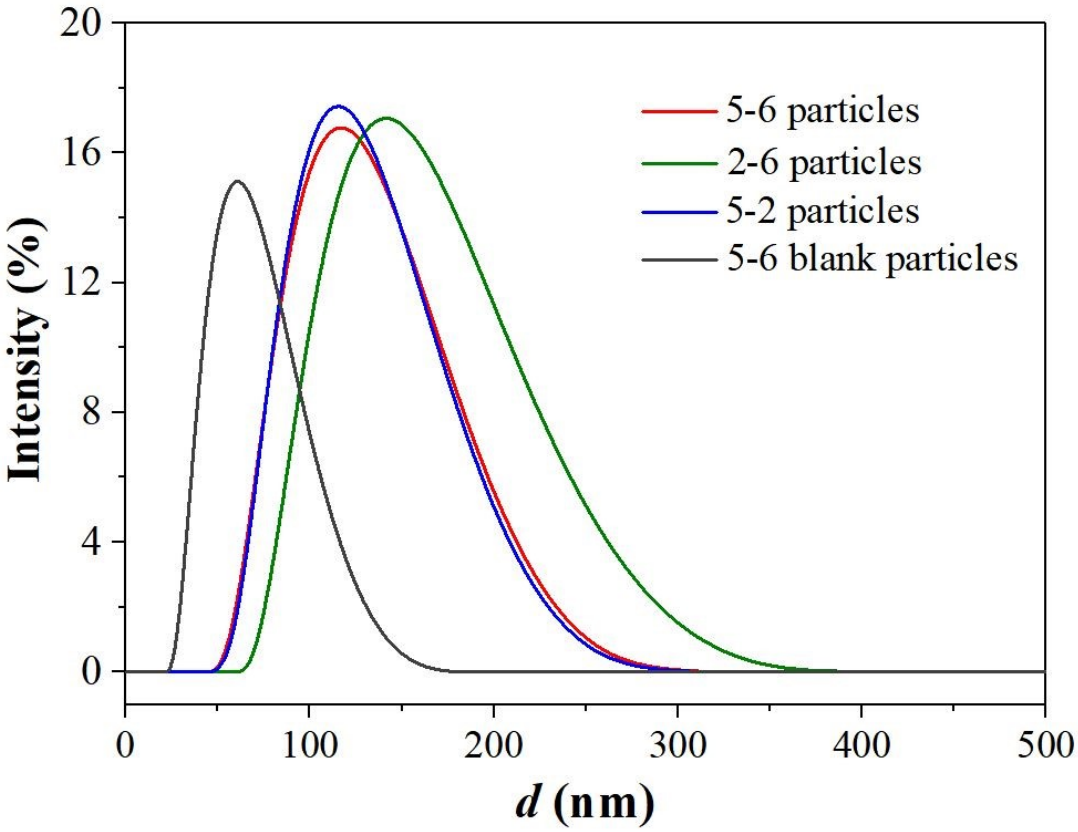

Fig. 6. Particle size and distribution of drug-loaded and blank copolymer particles.

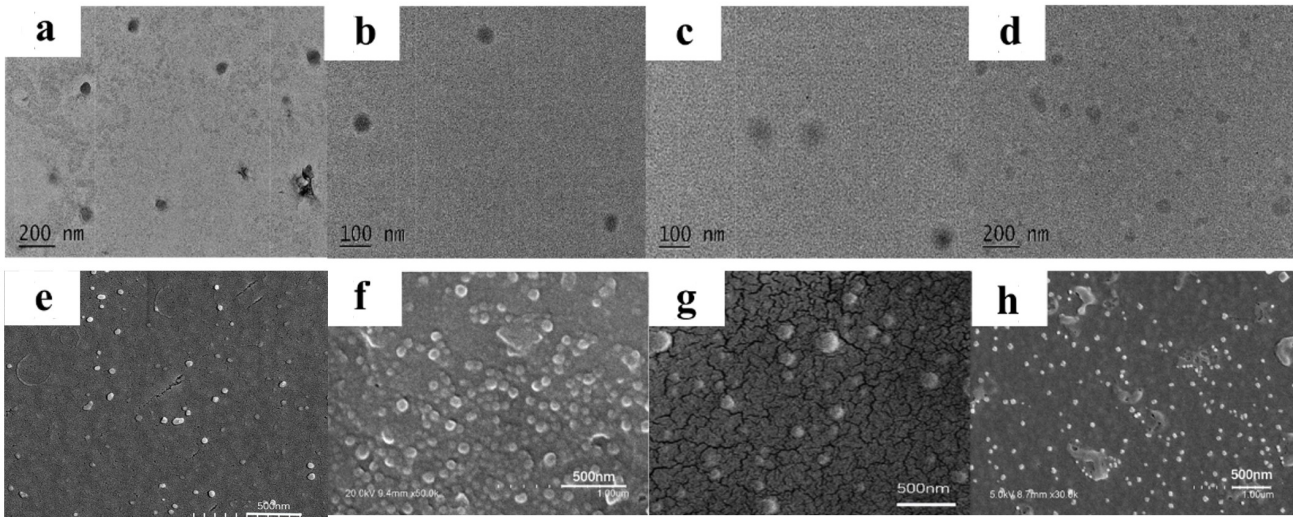

Fig. 7. TEM a-d and SEM e-h images of particles. (a,e) 5-6 particles; (b,f) 2-6 particles; (c,g) 5-2 particles; (d,h) 5-6 blank particles. Abbreviation: TEM, transition electron microscopy; SEM, scanning electron microscopy.

g/L, 1.0 $\times$ 10^{-3} g/L, 2.1 $\times$ 10^{-3} g/L, 2.5 $\times$ 10^{-3} g/L, respectively. The CMC values of the PTX-loaded particles were lower than those of the blank particles. This could be attributed to the hydrophobicity of PTX, which helps stabilize the particles. 5-6 particles and 2-6 particles with the same PLA segment length were compared, and the CMC value of 5-6 particles (1.4 $\times$ 10^{-3} g/L) was higher than that of 2-6 particles (1.0 $\times$ 10^{-3} g/L). This is because 5-6 particles have a higher molecular weight of MPEG, indicating stronger hydrophilicity. The stronger the hydrophilicity of the chain segment, the more difficult it is to form micelles. On comparing the CMC value of 5-6 particles (1.4 $\times$ 10^{-3} g/L) with 5-2 particles (2.1 $\times$ 10^{-3} g/L), particles with longer PLA segments have smaller CMC values when

Table 2. Theoretical total drug loading efficiency (TTLE) of PTX for the three particles.

	2-6 particles	5-2 particles	5-6 particles	5-6 blank particles
TTLE (%)	20.11	11.65	17.22	0.0

Table 3. Physical loading and chemical loading of drug-loaded particles.

Drug loading ratio	5-6 particles	5-2 particles	2-6 particles
Physical embedding method (%)	5.94	4.89	5.74
Chemical embedding method (%)	94.06	95.11	94.26

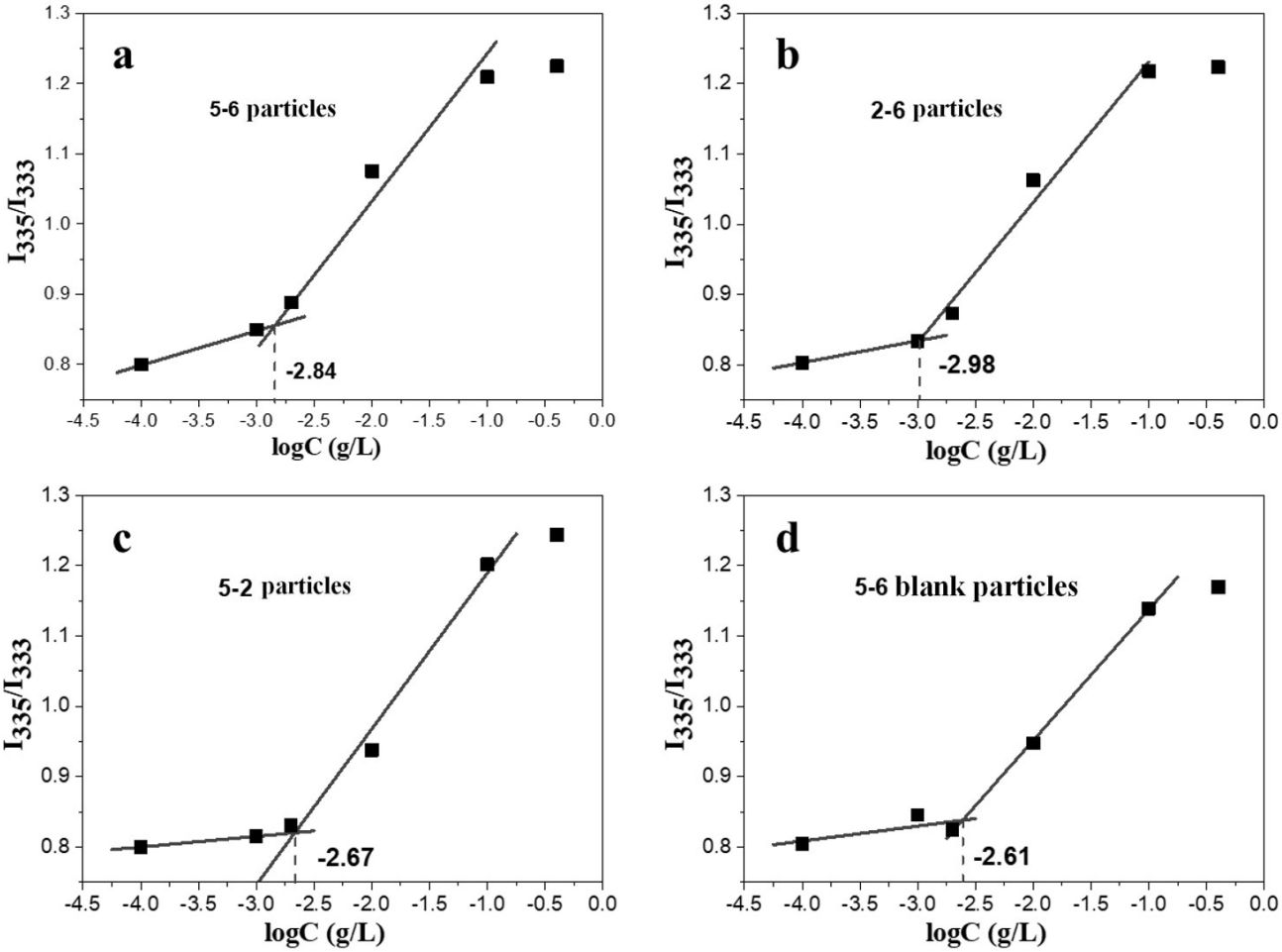

Fig. 8. Curves of maximum excitation peak intensity ratio I335 nm/I333 nm of micellar aqueous solution on the logarithm of concentration. (a) 5-6 particles. (b) 2-6 particles. (c) 5-2 particles. (d) 5-6 blank particles.

the length of the MPEG hydrophilic segment is the same. Longer PLA segments lead to enhanced hydrophobicity of particles, and hydrophobic interactions facilitate the formation of particles and decrease the CMC.

4.4 *In vitro* release studies of particles

As shown in Fig. 9 and Table 4, 5-2 particles had the largest cumulative PTX release percentages of 52.0% at 216 h. The cumulative release rate reached 20%–30% of the drug-loaded particles in the first 50 h, meeting the clinical need for achieving an effective blood concentration of 0.01 μM–0.1 μM within a short period, ranging between 8.54 μg/L and 85.4 μg/L in the present study. The drug showed a sustained and approximately linear release during subsequent release experiments, with a cumulative release of 37%–52% at 216 h. The release process was gradual with no sudden release. This controlled release effect can be attributed to the chemical linking between PTX and PLA, indicating that PTX can be released only through hydrolysis and the rupture of chemical bonds. Furthermore, the low CMC, based on the analysis in Section 4.3, renders the particles more stable, and the drug release is more sustained.

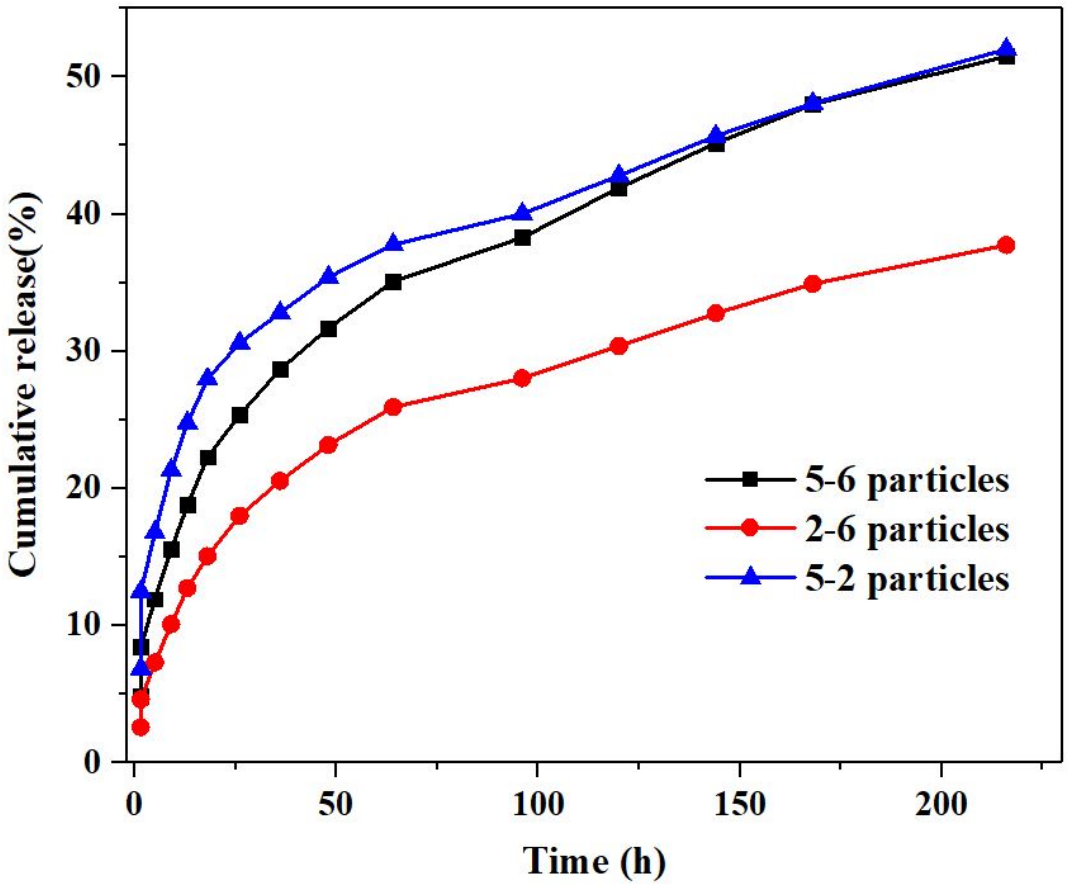

Fig. 9. Cumulative release percentage-release time curve of the *in vitro* release of 5-2, 5-6, and 2-6 particles at 216 h.

Table 4. Cumulative PTX release percentages at 216 h.

	5-6 particles	5-2 particles	2-6 particles
Release	51.5%	52.0%	37.7%

By comparing 5-6 particles with 2-6 particles, we observed that 5-6 particles presented a faster release of PTX than 2-6 particles. This may be attributed to the improved hydrophilicity of micellar nanospheres with longer MPEG segments. Improved hydrophilicity promotes hydrolysis of ester bonds between PTX and PDLA, facilitating the release of PTX. On comparing 5-6 particles with 5-2 particles, we found that the molecular weight of PLA minimally influenced the release rate. Thus, increasing the molecular weight of MPEG promoted the release of PTX.

The performances of the different types of PTX-loaded particles are listed in Table 5 (Ref. [30, 32, 46–49]) [46–51]. In the present study, relatively high loading efficiency and controlled release of PTX were achieved by preparing biodegradable PLA-based particles. Moreover, the amount of PTX loaded can be adjusted by modulating the PLLA chain length, and the release rate can be adjusted by adjusting the chain length of the MPEG in the MPEG-PLLA segment.

4.5 Tumor cell inhibition tests

Cell viability, excessive ROS generation, increase in mitochondrial depolarization, and cellular uptake of drugs were used to characterize the tumor cell inhibitory effects of PTX and PTX-loaded particles (Fig. 10).

4.5.1 Cell viability

As shown in Fig. 10a, PTX significantly decreased cell viability at 0.05 mg/L and higher concentrations. And 5-6 particles, 2-6 particles, and 5-2 particles decreased cell viability at 0.1 mg/L, 0.5 mg/L and 0.2 mg/L, respectively. At a concentration of 0.6 mg/L and lower, PTX induced greater cytotoxicity than the drug-loaded particles due to its burst release effect, which is undesirable in clinical applications. 5-6 particles and 5-2 particles induced higher cytotoxicity than PTX and 2-6 particles at concentrations above 0.8 mg/L with increasing exposure concentrations, demonstrating the controlled release process of drug-loaded particles.

4.5.2 Intracellular reactive oxygen species (ROS) level

Excessive ROS generation, an important indicator for monitoring cancer cells, can induce cell damage by destroying cellular proteins, lipids, and nucleic acids, affecting normal cellular signaling pathways and gene reg-

Table 5. Performance comparison of PTX-loaded particles formulated in the present study and PTX particles in the literature.

	PTX loading method	Particle size (nm)	CMC (g/L)	Release rate	Maximum drug load (%)
	Click chemistry of azide-alkynyl groups	10–100	/	65% at 72 h	23.2 [32]
Chemical methods	Ester bond	180–210	2.5×10^{-3}	/	16.0 [46]
	Ester bond	130	6.3×10^{-4}	50–55% at 216 h	10.0 [47]
	Lipophilicity of PTX	$2–3 \times 10^{3}$	/	/	10.8 [48]
Physical methods	Lipophilicity of PTX	96	0.8×10^{-3}	95–100% at 45 h	10.6 [30]
	Lipophilic of PTX	/	/	74–88% at 24 h	4.6 [49]
Particles in this paper	Ester bond	110–130	$1.0–2.5 \times 10^{-3}$	37–52% at 216 h	20.11

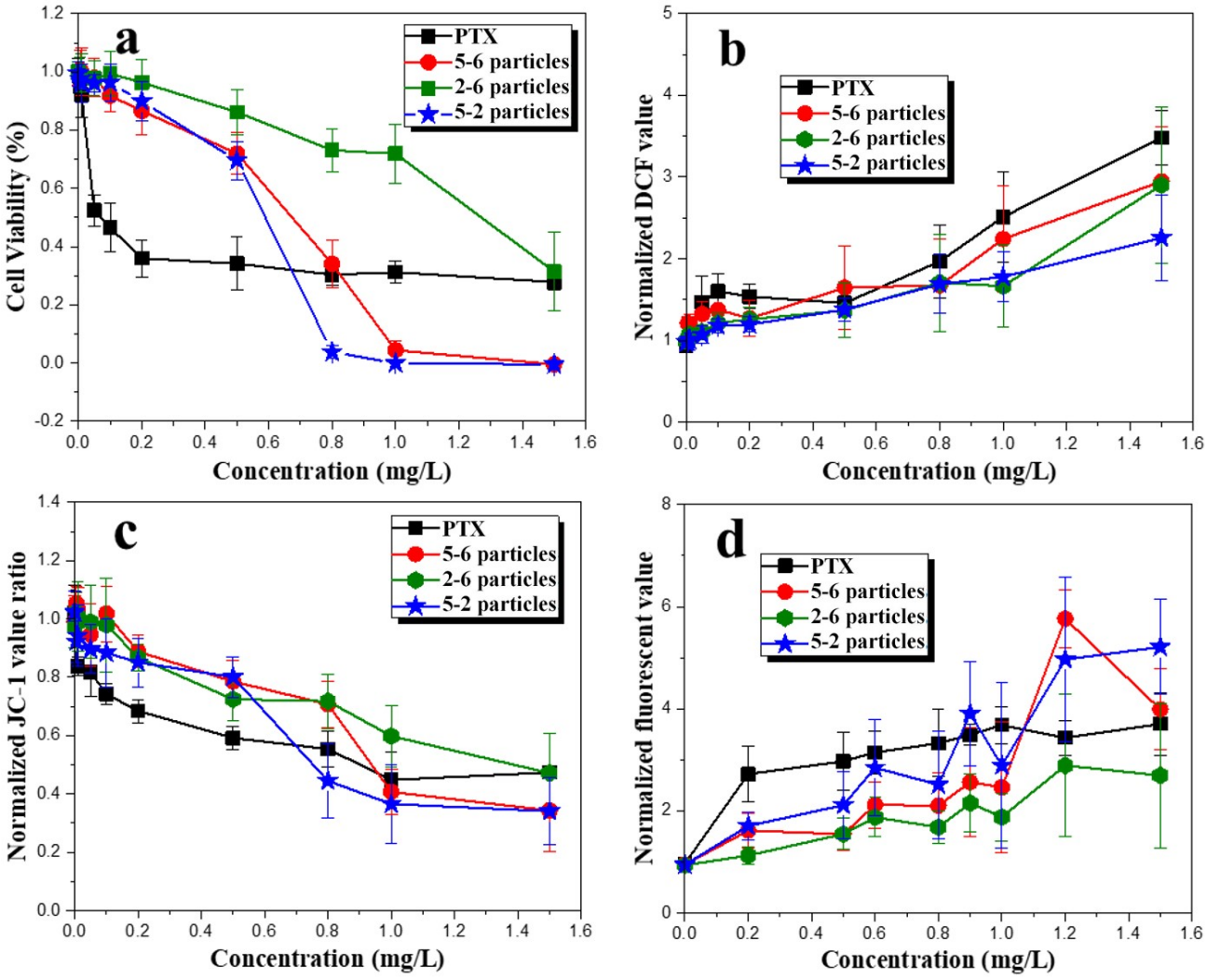

Fig. 10. (a) Cell viability, (b) normalized DCF fluorescence values, (c) mitochondrial membrane potential, and (d) normalized LysoTracker fluorescence values after 24 h exposure to PTX, 5-6 particles, 2-6 particles, and 5-2 particles.

ulation [50]. Intracellular ROS generation was measured using DCF fluorescence (Fig. 10b). Following exposure to PTX and PTX-loaded particles, intracellular ROS generation significantly increased. The lowest effective concentration of ROS generation for PTX and three drug-loaded particles were 0.05 mg/L and 0.5 mg/L.

4.5.3 Cell Apoptosis

The increase in mitochondrial depolarization was determined by the decrease in the red/green fluorescence intensity ratio (Fig. 10c). PTX and other particles all individually decreased the red/green ratio of JC-1 value ratio at 0.01 mg/L, 0.5 mg/L, and higher concentrations, indicating the occurrence of mitochondrial depolarization and potential cell apoptosis.

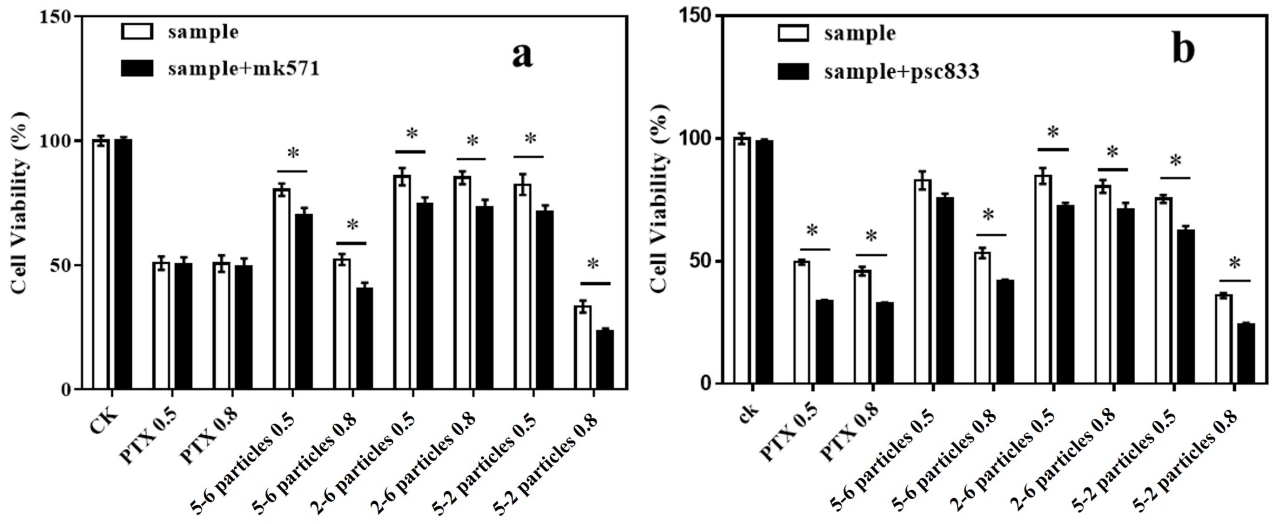

Fig. 11. Cell viability comparison with and without positive inhibitors. (a) MK571 as a positive inhibitor; (b) psc833 as a positive inhibitor.

4.5.4 Cell uptake of drugs

The cellular uptake of drugs was measured using the cell dye LysoTracker, which can indirectly determine the number of lysosomes (Fig. 10d). The results showed that exposure to PTX and drug-loaded particles significantly increased the number of lysosomes in HeLa cells. For PTX, the lowest effective concentration was 0.2 mg/L. For 5-6 particles, 2-6 particles, and 5-2 particles, the lowest effective concentrations were 0.6 mg/L, 0.5 mg/L, and 0.5 mg/L, respectively.

Generally, the lowest effective concentrations for the three particles are 0.5 mg/L, approximately. Furthermore, 2-6 particles caused lower cytotoxicity than 5-6 particles and 5-2 particles, which might be attributed to the lower release percentage (Table 4) and larger size (Fig. 6), which limits the number of drugs that enter the cell.

4.5.5 Membrane Transporter Activity

In the present study, MK571 and psc833, inhibitors of MRPs and P-gp transporter activity, were selected as positive controls. According to the significance test results ($P < 0.001$), the addition of MK571 did not influence the cytotoxicity of PTX alone (Fig. 11a). Moreover, PTX altered cell viability by inhibiting P-gp, whereas the three PTX-loaded micelles inhibited P-gp and MRP, indicating that P-gp is a transporter for PTX and drug-loaded micelles (Fig. 10b). However, MRP is not a PTX transporter.

CAM is a substrate of ABC transporters [51] and can be metabolized into calcein, which is not an ABC transporter substrate and is fluorescent; thus, it gets trapped in the cytoplasm. If the activity of ABC transporters is inhibited, calcein tends to accumulate, increasing the fluorescence values. The results of CAM accumulation induced by carrier material of PTX, PTX, 5-6 particles, 2-6 particles, and 5-2 particles exposure in HeLa cells are shown in Fig. 12.

When the carrier material is exposed to cells alone, CAM accumulation does not occur (Fig. 12a). Exposure of HeLa cells to PTX, 5-6 particles, 2-6 particles, and 5-2 particles increased the fluorescence values of CAM (Fig. 12c–e), indicating inhibition of ABC transporter activity. Furthermore, PTX, 5-6 particles, 2-6 particles, and 5-2 particles showed highly statistically significant differences ($P < 0.001$) at 0.8 mg/L, 0.8 mg/L, 0.5 mg/L, and 0.8 mg/L, respectively, meaning the lowest concentrations at which CAM accumulated was 0.8 mg/L, 0.8 mg/L, 0.5 mg/L, and 0.8 mg/L.

It could be postulated that when the drug-loaded particles enter cells, they are engulfed by lysosomes (Fig. 13), releasing PTX from the loading materials. The drug and drug-loaded particles entering cells induce oxidative stress by disturbing the balance between oxidant and antioxidant processes, such as the glutathione system. Subsequently, the generated ROS destroy the mitochondria and stimulate the production of lysosomes, inhibit cancer cell proliferation, and promote apoptosis.

5. Conclusions

This is the first study to propose a method for combining PTX-PDLA-PTX and MPEG-PLLA to prepare MPEG-SCPLA-PTX drug-loaded particles via a combination of chemical embedding and stereocomplexation. The average particle size was approximately 100 nm, which is suitable for human administration. Its low CMC ($1.0–2.5 \times 10^{-3}$) rendered it more stable and long-lasting in body fluid post dilution. In the simulated human environment, the cu-

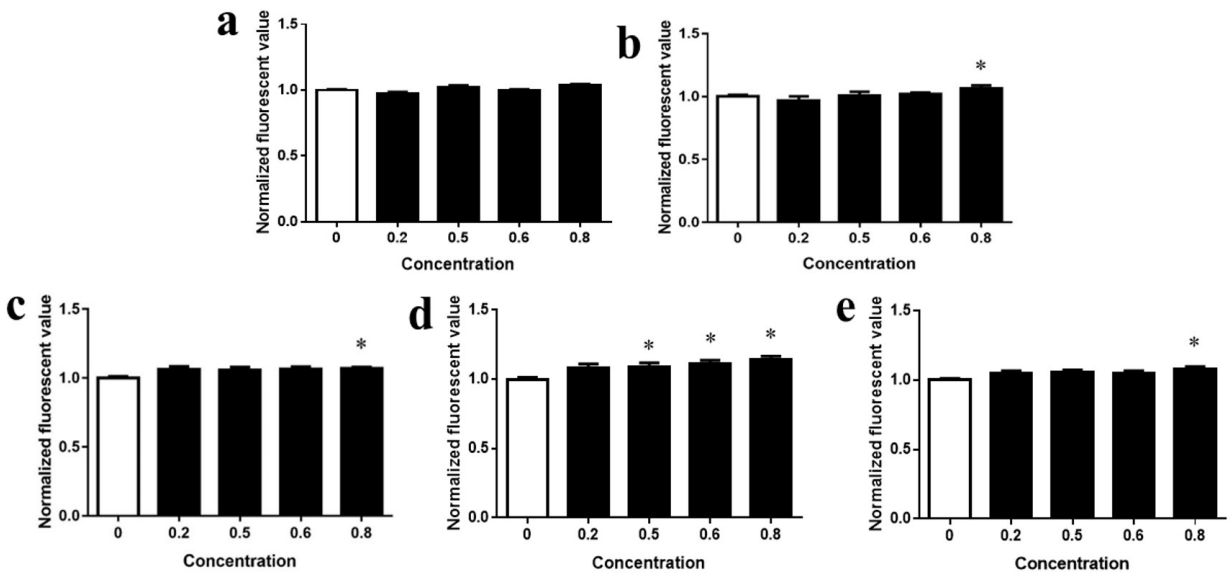

Fig. 12. Relative CAM fluorescence of (a) carrier material; (b) PTX; (c) 5-6 particles; (d) 2-6 particles; and (e) 5-2 particles. Abbreviation: CAM, calcein-AM; PTX, paclitaxel.

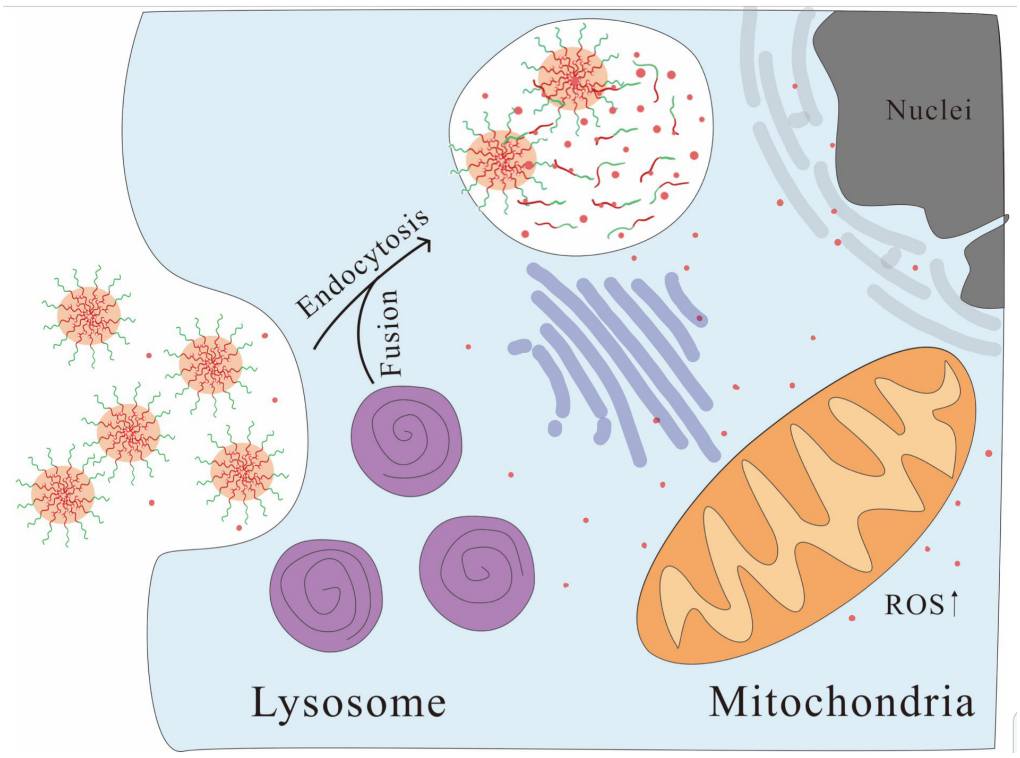

Fig. 13. Controlled release of PTX by MPEG-SCPLA-PTX particles in HeLa cells.

mulative release percentages of PTX from 5-6 particles, 2-6, and 5-2 particles were 51.5%, 37.7%, and 52.0% in 216 h, respectively. The entire release process was relatively gentle without burst release, meeting the requirements for sustained release. Moreover, the drug loading rate of 2-6 was 20.11%, which was as high as those observed with other methods. The PTX loading rate can be regulated by changing the lengths of PDLA and PLLA in the copolymer. Moreover, the tumor inhibition effect was better than that of PTX alone. In summary, the bio-based MPEG-SCPLA-PTX exhibiting a high PTX loading rate and controlled release performance is a promising macromolecular carrier for PTX.

6. Author contributions

SC conceived and designed the experiments; SC, YW performed the experiments; SC, YW, BW, WJ analyzed the data; WJ and QZ contributed reagents and materials.

7. Ethics approval and consent to participate

Not applicable.

8. Acknowledgment

Authors' are very grateful to Miss Jing Yu for her assistance in the Tumor cell experiment.

9. Funding

This work was supported by the National Natural Science Foundation of China (NSFC) (21304045).

10. Conflict of interest

The authors declare no conflict of interest.

11. References

[1] Barani M, Bilal M, Sabir F, Rahdar A, Kyzas GZ. Nanotechnology in ovarian cancer: Diagnosis and treatment. Life Sciences. 2021; 266: 118914.

[2] Zhang Y, Wang YY, Xue J. Paclitaxel inhibits breast cancer metastasis via suppression of Aurora kinase-mediated cofilin-1 activity. Experimental and Therapeutic Medicine. 2018; 15: 1269–1276.

[3] Luo B, Wu X, Feng Y, Zheng H, Zhang Q, Liang X, *et al*. Nuclear her2 contributes to paclitaxel resistance in breast cancer cells. Anti-Cancer Drugs. 2021; 32: 709–716.

[4] Okada T, Okamoto I, Sato H, Ito T, Miyake K, Tsukahara K. Efficacy and Safety of Paclitaxel Combined with Cetuximab for Head and Neck Squamous Cell Carcinoma. *in Vivo*. 2021; 35: 1253–1259.

[5] Riestra-Ayora J, Sanchez-Rodriguez C, Palao-Suay R, Yanes-Diaz J, Martin-Hita A, Aguilar MR, *et al*. Paclitaxel-loaded polymeric nanoparticles based on alpha-tocopheryl succinate for the treatment of head and neck squamous cell carcinoma: *in vivo* murine model. Drug Delivery. 2021; 28: 1376–1388.

[6] Bai Z, Ding N, Ge J, Wang Y, Wang L, Wu N, *et al*. Esomeprazole overcomes paclitaxel-resistance and enhances anticancer effects of paclitaxel by inducing autophagy in a549/Taxol cells. Cell Biology International. 2021; 45: 177–187.

[7] Kim J, Park Y. Improved Antitumor Efficacy of Hyaluronic Acid-Complexed Paclitaxel Nanoemulsions in Treating Non-Small Cell Lung Cancer. Biomolecules & Therapeutics. 2017; 25: 411–416.

[8] Guizhou G, Shenghao J, Nanni X, Wanzuo J, Zheng L. Study on extraction of taxol from taxus cuspidata by supercritical CO_2 fluid. Chemical Engineering. 2018; 46: 9–12.

[9] Ghosh B, Biswas S. Polymeric micelles in cancer therapy: State of the art. Journal of Controlled Release. 2021; 332: 127–147.

[10] Liu J, Liang N, Li S, Han Y, Yan P, Kawashima Y, *et al*. Tumor-targeting and redox-sensitive micelles based on hyaluronic acid conjugate for delivery of paclitaxel. Journal of Biomaterials Applications. 2020; 34: 1458–1469.

[11] Gradishar WJ. Albumin-bound paclitaxel: a next-generation taxane. Expert Opinion on Pharmacotherapy. 2006; 7: 1041–1053.

[12] Tarr B, Sambandan T, Yalkowsky SH. A new parenteral emulsion for the administration of taxol. Pharmaceutical Research. 1987; 4: 162–165.

[13] Symonds RP, Gourley C, Davidson S, Carty K, McCartney E, Rai D, *et al*. Cediranib combined with carboplatin and paclitaxel in patients with metastatic or recurrent cervical cancer (CIRCCa): a randomised, double-blind, placebo-controlled phase 2 trial. the Lancet Oncology. 2015; 16: 1515–1524.

[14] Miao Y, Chen M, Zhou X, Guo L, Zhu J, Wang R, *et al*. Chitosan oligosaccharide modified liposomes enhance lung cancer delivery of paclitaxel. Acta Pharmacologica Sinica. 2021: 1–9.

[15] Karpuz M, Dogan A, Nemutlu E, Silindir-Gunay M, Ozer AY. Simultaneous Quantification of Paclitaxel and Vinorelbine Encapsulated in Theranostic Nanosized Liposomes. Journal of Analytical Chemistry. 2021; 76: 742–748.

[16] Varan G, Patrulea V, Borchard G, Bilensoy E. Cellular Interaction and Tumoral Penetration Properties of Cyclodextrin Nanoparticles on 3D Breast Tumor Model. Nanomaterials. 2018; 8: 67.

[17] Shen Q, Shen Y, Jin F, Du Y, Ying X. Paclitaxel/hydroxypropyl-beta-cyclodextrin complex-loaded liposomes for overcoming multidrug resistance in cancer chemotherapy. Journal of Liposome Research. 2020; 30: 12–20.

[18] Feng X, Yuan Y, Wu J. Synthesis and evaluation of water-Soluble paclitaxel prodrugs. Bioorganic & Medicinal Chemistry Letters. 2002; 12: 3301–3303.

[19] Li Y, Yang M, Zhao Y, Li L, Xu W. Preparation and in vitro evaluation of amphiphilic paclitaxel small molecule prodrugs and enhancement of oral absorption. European Journal of Medicinal Chemistry. 2021; 215: 113276.

[20] Munjal NS, Shukla R, Singh TR. Physicochemical characterization of paclitaxel prodrugs with cytochrome 3A4 to correlate solubility and bioavailability implementing molecular docking and simulation studies. Journal of Biomolecular Structure & Dynamics. 2021.

[21] Duan X, Li Y. Physicochemical Characteristics of Nanoparticles Affect Circulation, Biodistribution, Cellular Internalization, and Trafficking. Small. 2013; 9: 1521–1532.

[22] Owen SC, Chan DPY, Shoichet MS. Polymeric micelle stability. Nano Today. 2012; 7: 53–65.

[23] Yasugi K, Nagasaki Y, Kato M, Kataoka K. Preparation and characterization of polymer micelles from poly(ethylene glycol)-poly(d,l-lactide) block copolymers as potential drug carrier. Journal of Controlled Release. 1999; 62: 89–100.

[24] Ma Z, Haddadi A, Molavi O, Lavasanifar A, Lai R, Samuel J. Micelles of poly(ethylene oxide)-b-poly(epsilon-caprolactone) as vehicles for the solubilization, stabilization, and controlled delivery of curcumin. Journal of Biomedical Materials Research Part A. 2008; 86A: 300–310.

[25] Andima M, Costabile G, Isert L, Ndakala AJ, Derese S, Merkel OM. Evaluation of β-Sitosterol loaded PLGA and PEG-PLA nanoparticles for effective treatment of breast cancer: Preparation, physicochemical characterization, and antitumor activity. Pharmaceutics. 2018; 10: 232.

[26] Zhang L, Liu Z, Kong C, Liu C, Yang K, Chen H, *et al*. Improving Drug Delivery of Micellar Paclitaxel against Non-Small Cell Lung Cancer by Coloading Itraconazole as a Micelle Stabilizer and a Tumor Vascular Manipulator. Small. 2018; 14: 1802112.

[27] Ma C, Pan P, Shan G, Bao Y, Fujita M, Maeda M. Core–Shell Structure, Biodegradation, and Drug Release Behavior of Poly(lactic acid)/Poly(ethylene glycol) Block Copolymer Micelles Tuned by Macromolecular Stereostructure. Langmuir. 2015; 31: 1527–1536.

[28] Wang Q, Wei N, Liu X, Chang A, Qian Luo K. Enhancement of the bioavailability of a novel anticancer compound (acetyltanshinone IIA) by encapsulation within mPEG-PLGA nanoparticles: a study of formulation optimization, toxicity, and pharmacokinetics. Oncotarget. 2017; 8: 12013–12030.
[29] Han X, Chen D, Sun J, Zhou J, Li D, Gong F, *et al*. A novel cabazitaxel-loaded polymeric micelle system with superiorin vitrostability and long blood circulation time. Journal of Biomaterials Science, Polymer Edition. 2016; 27: 626–642.
[30] Chen L, Xie Z, Hu J, Chen X, Jing X. Enantiomeric PLA–PEG block copolymers and their stereocomplex micelles used as rifampin delivery. Journal of Nanoparticle Research. 2007; 9: 777–785.
[31] Yu Y, Zou J, Yu L, Ji W, Li Y, Law W, *et al*. Functional Polylactide-g-Paclitaxel–Poly(ethylene glycol) by Azide–Alkyne Click Chemistry. Macromolecules. 2011; 44: 4793–4800.
[32] Yu Y, Chen C, Law W, Mok J, Zou J, Prasad PN, *et al*. Well-Defined Degradable Brush Polymer–Drug Conjugates for Sustained Delivery of Paclitaxel. Molecular Pharmaceutics. 2013; 10: 867–874.
[33] Li W, Fan X, Wang X, Shang X, Wang Q, Lin J, *et al*. Stereocomplexed micelle formation through enantiomeric PLA-based Y-shaped copolymer for targeted drug delivery. Materials Science and Engineering: C. 2018; 91: 688–695.
[34] Yu B, Meng L, Fu S, Zhao Z, Liu Y, Wang K, *et al*. Morphology and internal structure control over PLA microspheres by compounding PLLA and PDLA and effects on drug release behavior. Colloids and Surfaces B: Biointerfaces. 2018; 172: 105–112.
[35] Portinha D, Bouteiller L, Pensec S, Richez A, Chassenieux C. Influence of Preparation Conditions on the Self-Assembly by Stereocomplexation of Polylactide Containing Diblock Copolymers. Macromolecules. 2004; 37: 3401–3406.
[36] Gao H, Tan Y, Guan Q, Cai T, Liang G, Wu Q. Synthesis, characterization and micellization of amphiphilic polyethylene-b-polyphosphoester block copolymers. RSC Advances. 2015; 5: 49376–49384.
[37] Nagasaki Y, Okada T, Scholz C, Iijima M, Kato M, Kataoka K. The Reactive Polymeric Micelle Based on an Aldehyde-Ended Poly(ethylene glycol)/Poly(lactide) Block Copolymer. Macromolecules. 1998; 31: 1473–1479.
[38] Liu D, Liu Z, Wang L, Zhang C, Zhang N. Nanostructured lipid carriers as novel carrier for parenteral delivery of docetaxel. Colloids and Surfaces B: Biointerfaces. 2011; 85: 262–269.
[39] George S, Lin S, Ji Z, Thomas CR, Li L, Mecklenburg M, *et al*. Surface Defects on Plate-Shaped Silver Nanoparticles Contribute to its Hazard Potential in a Fish Gill Cell Line and Zebrafish Embryos. ACS Nano. 2012; 6: 3745–3759.
[40] Setyawati MI, Yuan X, Xie J, Leong DT. The influence of lysosomal stability of silver nanomaterials on their toxicity to human cells. Biomaterials. 2014; 35: 6707–6715.
[41] Zhou Y, Lu N, Qiao C, Ni T, Li Z, Yu B, *et al*. FV-429 induces apoptosis and inhibits glycolysis by inhibiting Akt-mediated phosphorylation of hexokinase II in MDA-MB-231 cells. Molecular Carcinogenesis. 2016; 55: 1317–1328.
[42] Nam HY, Kwon SM, Chung H, Lee S, Kwon S, Jeon H, *et al*. Cellular uptake mechanism and intracellular fate of hydrophobically modified glycol chitosan nanoparticles. Journal of Controlled Release. 2009; 135: 259–267.
[43] Byrd IV TF, Hoang LT, Kim EG, Pfister ME, Werner EM, Arndt SE, *et al*. The microfluidic multitrap nanophysiometer for hematologic cancer cell characterization reveals temporal sensitivity of the calcein-am efflux assay. Scientific Reports. 2014; 4: 1–9.
[44] Shukla S, Schwartz C, Kapoor K, Kouanda A, Ambudkar SV. Use of Baculovirus BacMam Vectors for Expression of ABC Drug Transporters in Mammalian Cells. Drug Metabolism and Disposition. 2012; 40: 304–312.
[45] Pensec S, Leroy M, Akkouche H, Spassky N. Stereocomplex formation in enantiomeric diblock and triblock copolymers of poly(epsilon-caprolactone) and polylactide. Polymer Bulletin. 2000; 45: 373–380.
[46] Xie Z, Lu T, Chen X, Lu C, Zheng Y, Jing X. Triblock poly(lactic acid)-b-poly(ethylene glycol)-b-poly(lactic acid)/paclitaxel conjugates: Synthesis, micellization, and cytotoxicity. Journal of Applied Polymer Science. 2007; 105: 2271–2279.
[47] Xu X, Zhang X, Wang X, Li Y, Jing X. Comparative study of paclitaxel physically encapsulated in and chemically conjugated with PEG-PLA. Polymers for Advanced Technologies. 2009; 20: 843–848.
[48] Huang X, Zhang Y, Yin G, Pu X, Liao X, Huang Z, *et al*. Tumor-targeted paclitaxel-loaded folate conjugated poly(ethylene glycol)-poly(l-lactide) microparticles produced by supercritical fluid technology. Journal of Materials Science: Materials in Medicine. 2015; 26: 95.
[49] Jelonek K, Li S, Kaczmarczyk B, Marcinkowski A, Orchel A, Musiał-Kulik M, *et al*. Multidrug PLA-PEG filomicelles for concurrent delivery of anticancer drugs—the influence of drug-drug and drug-polymer interactions on drug loading and release properties. International Journal of Pharmaceutics. 2016; 510: 365–374.
[50] Moloney JN, Cotter TG. ROS signalling in the biology of cancer. Seminars in Cell & Developmental Biology. 2018; 80: 50–64.
[51] Panieri E, Santoro MM. ROS homeostasis and metabolism: a dangerous liason in cancer cells. Cell Death & Disease. 2016; 7: e2253–e2253.

Supplementary material: Supplementary material associated with this article can be found, in the online version, at https://www.fbscience.com/Landmark/articles/10.52586/4964.

Keywords: Paclitaxel; MPEG-PLLA; Stereocomplex; Nanoparticles; Controllable drug loading

Send correspondence to: Wei Jiang, State Key Laboratory of Pollution Control and Resources Reuse, National Engineering Research Center for Organic Pollution Control and Resource Reuse, School of the Environment, Nanjing University, 210023 Nanjing, Jiangsu, China, E-mail: jiangwei@nju.edu.cn